INTERNATIONAL JOURNAL FOR NUMERICAL METHODS IN ENGINEERING
Int. J. Numer. Meth. Engng 2008; **73**:427–445
Published online 12 June 2007 in Wiley InterScience (www.interscience.wiley.com). DOI: 10.1002/nme.2080

Coupling boundary elements to a raytracing procedure

S. Hampel[1], S. Langer[1,2,*,†] and A. P. Cisilino[3]

[1]*Institute of Applied Mechanics, Technical University Braunschweig, Spielmannstr. 11, 38106 Braunschweig, Germany*
[2]*Institute of Applied Mechanics, Technical University Clausthal, Adolph-Roemer-Str. 2a, 38678 Clausthal-Zellerfeld, Germany*
[3]*Welding and Fracture Division, Faculty of Engineering, University of Mar del Plata, INTEMA, Av. Juan B. Justo, Mar del Plata 4302-7600, Argentina*

SUMMARY

Typical outdoor sound propagation problems are governed by two principal phenomena: (i) diffraction in the vicinity of the noise source due to objects such as buildings or insulation barriers, and (ii) refraction at long distances from the source as a consequence of the effects of wind and temperature. The boundary element method (BEM) is well suited to account for the diffraction phenomena in the near field, while the raytracing method based on geometrical acoustics is more effective to deal with the refraction phenomena.

In this paper, a new approach is presented which couples the direct BEM and a raytracing model in order to combine their advantages. Two alternative coupling procedures are developed, one is using a singular indirect BEM and the other is based on the method of fundamental solutions (MFS).

The direct boundary element model is applied first for solving the near field and computing the sound pressure along an auxiliary interface which limits the near field extent. Then, a singular indirect BEM or MFS is used to find the intensities of a number of point sources which produce the same sound pressure on the interface to that resulting from the near-field analysis. Finally, the point sources are the input data for the raytracing model of the far field.

A 3D implementation of the proposed method is finally applied to an outdoor sound propagation problem. Copyright © 2007 John Wiley & Sons, Ltd.

Received 20 October 2006; Revised 20 February 2007; Accepted 23 March 2007

KEY WORDS: BEM; raytracing; hybrid method; outdoor sound propagation; acoustics; coupling

*Correspondence to: S. Langer, Institute of Applied Mechanics, Technical University Braunschweig, Spielmannstr. 11, 38106 Braunschweig, Germany.
†E-mail: s.langer@tu-clausthal.de, s.langer@tu-bs.de

Contract/grant sponsor: DFG—Deutsche Forschungsgemeinschaft; contract/grant number: GRK-432
Contract/grant sponsor: ELBENet—Europe Latin America Boundary Element Network; contract/grant number: ALFA II-0357-FA-FCD-FI

1. INTRODUCTION

This paper focuses on numerical methods to study outdoor sound propagation. Various phenomena have to be considered when studying this problem, namely reflection, absorption, diffraction, refraction, and scattering. All these phenomena have been well known for a long time, and plenty of material can be found in the literature. General overviews on the physics of the problem are for example available in [1, 2], while [3, 4] provide details about the modelling aspects.

The finite element method (FEM) is widely used in structural dynamics. Besides, it is also well suited to study interior sound fields [5] and the sound–structure interaction [6]. But FEM possesses a disadvantage when dealing with infinite domains, it does not fulfil the Sommerfeld radiation condition [7], and thus, there can be artificial reflections at the remote exterior FE-discretized boundary coming back into the model domain. Alternative numerical methods for solving sound propagation problems are finite difference (FD) schemes. FD schemes have been successfully used to model realistic wind fields [8, 9], but like the FEM, they also have the drawback of inducing artificial reflections along the remote exterior boundary when solving problems with infinite domains. Besides, FD possess the disadvantage of their relatively high computational costs when compared to other methods. Raytracing procedures are widely used in room acoustics where sound rays propagate straightforwardly. On the other hand, special raytracing methods account for refraction and hence the curving of the ray path. There are various time domain raytracing procedures that consider refraction (see e.g. [10, 11]). Salomons describes a raytracing procedure considering refraction in frequency domain in [12] which is necessary for the solution of outdoor sound propagation problems. Another effective numerical tool for the solution of acoustical problems is the boundary element method (BEM) [13–16]. Formulations of the BEM to study sound propagation in a uniform flow are presented in [17–19]. More recently, a promising development is the so-called fast boundary element algorithm capable of enhancing the performance of BEM significantly (see e.g. [20]). Finally, the method of fundamental solutions (MFS) has also been successfully applied to acoustical problems; an overview on the MFS can be found in [21] while further developments of the method to acoustics can be found in [22]. A key issue of the MFS is the positioning of the sources. This topic is discussed in [23] and will be considered later in this paper.

Hence, a number of numerical methods have been developed for different purposes. However, no universal method exists that is capable of solving a large variety of problems. In order to overcome the drawbacks proprietary to many methods in their applications, hybrid methods have gained importance in recent research. Thus, two or more methods are combined in order to make use of their respective advantages and to overcome their disadvantages. The coupling of FEM and BEM is very popular and for instance successfully applied to study sound transmission [6] or acoustic radiation in a subsonic non-uniform flow [24]. Furthermore, in [25] BEM is coupled to a parabolic equation (PE) method. PE can consider a non-homogeneous atmosphere but no diffraction.

In this paper, a hybrid procedure is presented that is well suited to study outdoor sound propagation: boundary elements coupled with a raytracing procedure.

Noise often occurs in a domain where many objects such as buildings or sound insulation walls scatter the sound. Hence, diffraction prevails and consequentially needs to be considered in developing a suitable solution procedure. The use of BEM for acoustics in the frequency domain is based on an integral formulation of a wave equation. Thus, wave effects like diffraction are implicitly taken into account. However, to study the effects of noise on a sound receiver located

DOI: 10.1002/nme

far away from the source, the refraction effect caused by a wind or temperature profile cannot be neglected. Raytracing may be preferable for such an application because refraction can be implemented more easily than in BEM. Indeed, the principal limitation of the BEM in this sense is its restriction to deal with homogeneous domains.

Hence, in the method proposed in this paper, the direct BEM formulation is applied in the near field while a raytracing procedure is used to analyse the far field. As the sound propagation is considered in the frequency domain, a special raytracing algorithm is implemented. Two alternative procedures for the BEM-raytracing coupling are developed: the first one is using the indirect BEM while the other one is based on the MFS. Finally, an example problem shows the successful application of proposed methodology to outdoor acoustics.

2. THE BOUNDARY ELEMENT METHOD

2.1. General aspects

The direct BEM formulation for acoustics in the frequency domain is based on an integral formulation of the Helmholtz equation, which is the scalar wave equation transformed into the frequency domain using a time-harmonic approach for the pressure (see, e.g. [15, 16]). Since the BEM solves the wave equation, all phenomena related to the wave nature of the problem are considered implicitly. Particularly diffraction can be represented adequately. For instance, in the case of a rigid sound barrier, BEM is capable of exactly determining the sound field in the geometrical shadow zone due to diffraction around the top of the barrier.

The so-called fundamental solution plays a key role in the BEM formulation. It represents the pressure distribution in the free space due to a harmonically exciting point source. In this case, a fundamental solution G is defined to fulfil the inhomogeneous Helmholtz equation

$$\nabla^2 G + k^2 G = -\delta(\mathbf{x} - \boldsymbol{\xi}) \tag{1}$$

where k is the wave number and the argument of the Dirac distribution is the distance from the field point at location $\mathbf{x}$ to the source point at $\boldsymbol{\xi}$.

Following standard procedures [16], the boundary integral equation of the Helmholtz equation for a domain Ω with boundary Γ can be derived to result

$$c(\boldsymbol{\xi})\, p(\boldsymbol{\xi}) + \int_\Gamma p\, \frac{\partial G}{\partial n}\, \mathrm{d}\Gamma = \int_\Gamma \frac{\partial p}{\partial n}\, G\, \mathrm{d}\Gamma - \int_\Omega a G\, \mathrm{d}\Omega \tag{2}$$

where the factor c depends on the local shape of the boundary at the position of the source point $\boldsymbol{\xi}$. The primary field variables in Equation (2) are the pressure p and its normal derivative $\partial p/\partial n$ which represents the flux on the boundary. The symbol a denotes a source intensity distribution.

For a point source at $\boldsymbol{\xi}_a$ with sound intensity a_0—i.e. $a(\boldsymbol{\xi}) = a_0 \delta(\boldsymbol{\xi} - \boldsymbol{\xi}_a)$—the domain integral in Equation (2) can easily be evaluated:

$$\int_\Omega a(\boldsymbol{\xi}) G(\mathbf{x}, \boldsymbol{\xi})\, \mathrm{d}\Omega_x = \int_\Omega a_0\, \delta(\boldsymbol{\xi} - \boldsymbol{\xi}_a) G(\mathbf{x}, \boldsymbol{\xi})\, \mathrm{d}\Omega_x = a_0\, G(\boldsymbol{\xi}, \boldsymbol{\xi}_a) \tag{3}$$

Note that after replacing Equation (3) into Equation (2) a boundary-only equation results. The BEM consists in solving the resultant boundary integral equation numerically. With this purpose, the model boundary is discretized using boundary elements and a point collocation scheme is applied

DOI: 10.1002/nme

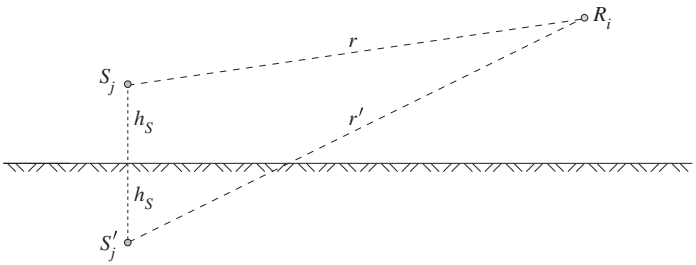

Figure 1. Geometry of source–receiver distance in the case of a half-space.

to obtain a linear system of equations. After replacing the problem boundary conditions (known pressures and fluxes acting on the model boundary) the system can be conveniently manipulated to solve the unknown pressures and fluxes on the boundary. The boundary-only discretization of the BEM is one of the main features of the method, in contrast to domain discretization methods as it is the case of FEM.

The fundamental solution for the free space can be extended for the case of an infinite half-space by adding a second term, which represents the effect of a mirror image source:

$$G(\mathbf{x}, \boldsymbol{\xi}) = \frac{1}{4\pi r} \mathrm{e}^{\mathrm{i}kr} + R \frac{1}{4\pi r'} \mathrm{e}^{\mathrm{i}kr'} \tag{4}$$

where $r = |\mathbf{x} - \boldsymbol{\xi}|$ is the distance from the original source to the receiver and r' is the distance from the mirror source to the receiver (Figure 1). R represents the reflection coefficient of the ground.

2.2. Implementation aspects

When using the BEM for exterior problems, no outer boundary of the domain has to be discretized, so that, the model discretization is limited to the geometry of the objects in the near field only. The Sommerfeld radiation condition is implicitly fulfilled and ensures that no reflections occur along the remote boundary [7]. The half-space fundamental solution (4) takes into account the ground reflections at the infinite plane.

The results of a BEM calculation are the pressure and flux distribution on the model boundary. Then, once the boundary solution is known, the sound pressure inside the domain Ω can be solved for any internal point $\boldsymbol{\xi}_i$ in a post-processing step by using

$$p(\boldsymbol{\xi}_i) = \int_\Gamma G(\mathbf{x}, \boldsymbol{\xi}_i) \frac{\partial p(\mathbf{x})}{\partial n} \, \mathrm{d}\Gamma - \int_\Gamma \frac{\partial G(\mathbf{x}, \boldsymbol{\xi}_i)}{\partial n} p(\mathbf{x}) \, \mathrm{d}\Gamma, \quad \boldsymbol{\xi}_i \in \Omega \tag{5}$$

The details about the BEM implementation can be found e.g. in [26].

3. THE RAYTRACING METHOD

3.1. General aspects

Raytracing methods neglect the wave character of sound and assume that sound particles travel on sound rays from the source to the receiver. Depending on the geometry and the propagation

DOI: 10.1002/nme

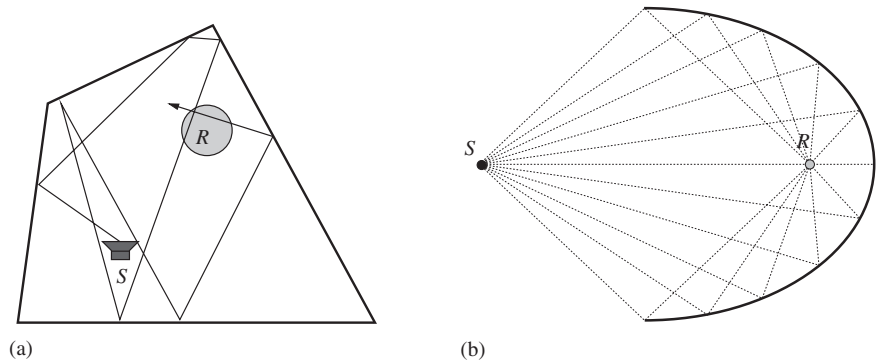

Figure 2. Examples of geometrical acoustics: (a) sound ray image for a homogeneous domain with receiver area R and (b) focusing of sound rays in the focal point R of an ellipse.

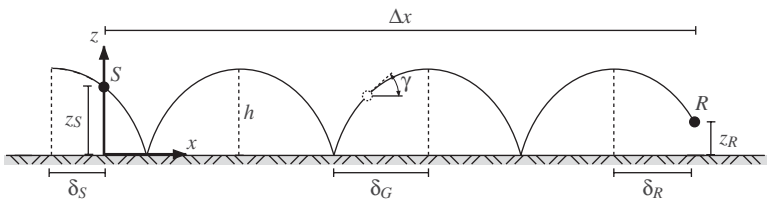

Figure 3. Sound ray path consisting of curved segments.

medium the ray paths are derived, which represent all possible ways a sound particle can take to reach the receiver. The contributions of the rays are finally added to get the total signal representing the sound pressure at the receiver. Simple reflection laws are applied when a sound ray hits an obstacle. Two examples of geometrical acoustics are shown in Figure 2.

The application of raytracing methods is suitable for high frequencies, which corresponds to short wavelengths. This is due to the fact that the sound wave in this case indeed behaves like sound rays. However, for low frequencies wave phenomena like diffraction appear. Raytracing methods are applied mostly for room acoustics, e.g. to design concert halls.

3.2. Semi-analytical ray model

A special ray method is the semi-analytical raytracing model of Salomons [12]. The Salomons method is formulated in the frequency domain, what makes it compatible with the introduced direct BEM formulation. The model considers a stationary vertical profile of effective sound speed, which is constant along the propagation direction. The linear profile $c_{\text{eff}}^{\text{lin}}(z)$ is given as

$$c_{\text{eff}}^{\text{lin}}(z) = c_0 + a_{\text{prof}}\, z \tag{6}$$

where a_{prof} is the gradient of the sound speed profile. Each ray shows a certain characteristic due to the uniform atmosphere between source and receiver: it consists of curved segments which repeat in the horizontal direction, if the ray is multiple reflected at the ground (see Figure 3). From the wave speed profile in Equation (6) the curved sound path can be derived. This is done by using

DOI: 10.1002/nme

Snell's law which relates the gradient in the sound speed profile to the inclination angle $\gamma(z)$ (see Figure 3). The determination of the ray paths fitting between source and receiver positions requires considering the horizontal distances only. These are given in terms of h (the ray maximum height, see Figure 3) by

$$\delta_j(h) = \int_{z_j}^{h} \mathrm{d}x = \int_{z_j}^{h} \frac{\mathrm{d}z}{\tan\gamma(z)} \tag{7}$$

where the subscript j represents the variables S, G and R as depicted in Figure 3. Thus, δ_j stand for the horizontal distance at the source point δ_S, the horizontal half-length of a complete segment δ_G, and the horizontal distance at the receiver δ_R (see Figure 3). Similarly, z_j stand for the height of the source z_S, the height of the ground $z_G = 0$, and the height of the receiver z_R, respectively.

Adding up the contributions of all rays leads to the geometrical solution

$$p_{\mathrm{geom}} = a_S \sum_{m=1}^{M} A_m \mathrm{e}^{\mathrm{i}\phi_m} \tag{8}$$

where a_S is the complex source intensity of the point source. Each contribution results from the amplitude A_m and the phase ϕ_m, which can be determined as

$$A_m = f_m R_m^{N_m} \tag{9}$$

$$\phi_m = \omega t_m \tag{10}$$

The amplitude of the sound ray m depends on the so-called focus factor f_m, the reflection coefficient R_m and the number of reflections N_m. The focus factor is a special quantity in the model of Salomons. It describes the density of sound rays at a certain point compared to the density in homogeneous free space. The phase is derived from angular frequency ω and the travel time t_m from the source to the receiver.

It is worth noting that Equations (9) and (10) show the implicit dependence of the sound pressure with the wave speed (see Equation (6)). The wave speed enters in Equation (8) in terms of the travel time t_m via Equation (10). The travel time results from the travel path and the sound speed profile.

3.3. Implementation aspects

A raytracing model does not require performing any domain or boundary discretization, even when a half-space problem is considered. The plane ground is simply characterized by its reflection coefficient R, and the height over the ground is given by the coordinate z. Input data consist in point sources with complex intensity. If more than one source is prescribed, the total sound pressure results from the superposition of the single pressure fields.

4. COUPLING PROCEDURE

From the previous sections, it follows that no pre-defined interface between the two computation domains (the near field for the BEM analysis and the far field for the raytracing analysis) exists, because both of them extend to infinity. Thus, a suitable coupling method must be able to retrieve

DOI: 10.1002/nme

the pressure information from the BEM model and to transform it into equivalent point sources for the raytracing model.

Attending to the inherent characteristics of the raytracing method, a kind of weak coupling procedure is used in this work. Two alternative methods for the coupling procedure are presented in the following sections [27, 28].

4.1. Coupling by the indirect boundary element method

As no domain boundaries are defined explicitly, an artificial auxiliary interface Γ^{I} has to be chosen, where the coupling from BEM to the ray method takes place (see Figure 4). This interface separates the near field (BEM) from the far field (ray method). The interface is defined by means of an array of internal points at which the sound pressure is evaluated using Equation (5). Then, the interface Γ^{I} is discretized using a set of auxiliary elements and the pressure interpolated using their shape functions in order to compute a continuous pressure distribution along the complete interface. For the transformation of a pressure distribution into a discrete complex source intensity distribution, the indirect BEM is used. From the boundary integral equation, we get [13]

$$\int_{\Gamma^{\mathrm{I}}} G(\mathbf{x}, \boldsymbol{\xi}) a^*(\boldsymbol{\xi}) \, \mathrm{d}\Gamma_{\boldsymbol{\xi}} = \bar{p}(\mathbf{x}) \tag{11}$$

with known pressures $\bar{p}$ and unknown source intensities a^* along the interface Γ^{I}. In its discrete form Equation (11) results in a linear system of equations which serves for the calculation of the source intensities a^*. Note that in the frequency domain the source intensity a^* is complex value according to the complex sound pressure p. Finally, the source intensity is integrated over each individual interface element in order to obtain an equivalent point source (see Figure 5).

Two alternatives for the selection of the shape and the location of the auxiliary interface are explored. They are illustrated in Figure 6. The first one consists of a half-sphere (or a half-circle in 2D) around the near field which encloses the primary source and the obstacle (Figure 6(a)). The second alternative is a vertical plane (or a vertical line in 2D) which is placed beyond the obstacle (Figure 6(b)). Although an interface like the one in Figure 6(a) seems to be the more logical choice, it is not eligible for the proposed analyses. Following the procedure described above, the coupling procedure will deliver secondary (equivalent) sources along the interface. If there is an obstacle between these sources and the receiver (as in the case of several sources in Figure 6(a)) which influence the propagation significantly, the obstacle should be considered in the ray calculation. This analysis is beyond the capabilities of the raytracing method used in this

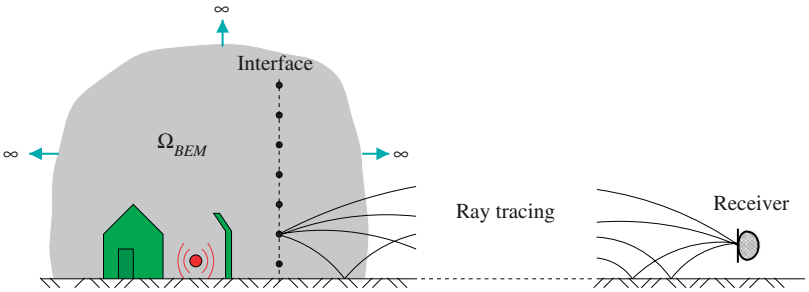

Figure 4. Sketch of the coupling at the auxiliary interface.

DOI: 10.1002/nme

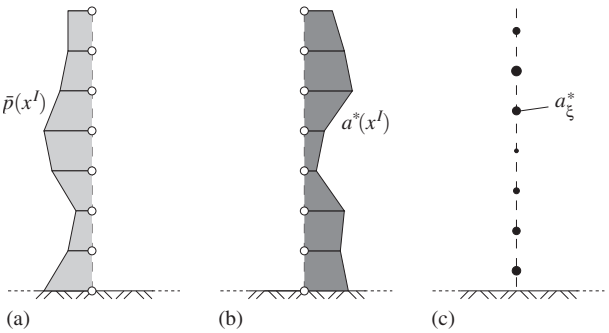

Figure 5. Scheme of transformation from pressure distribution to equivalent point sources: (a) pressure distribution from BEM calculation; (b) source intensity distribution from Equation (11); and (c) equivalent point sources by integration.

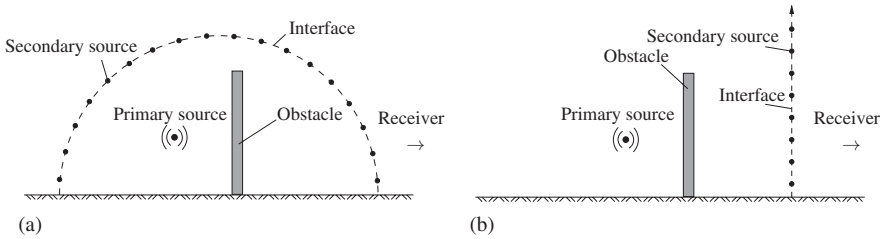

Figure 6. Different shapes of the auxiliary interface: (a) auxiliary interface as half-circle or sphere around the near field and (b) auxiliary interface as vertical line or surface between near field and far field.

work. For this reason, the shape and position of the interface have to be chosen such that there is no influence of the obstacles on the propagation from the secondary sources towards the receiver. Thus, second alternative for the interface is used in the following.

The proposed procedure is verified for a simple 2D problem like the one illustrated in Figure 6: a homogeneous half-space with a vertical barrier and with rigid ground and no refraction effects. A single BEM calculation involving both the near and the far field is used as reference solution. Apart from very small discretization errors, the BEM delivers a very accurate reference solution to which the solution of the hybrid method can be compared. In order to restrict the verification to the coupling procedure only (i.e. the raytracing is excluded from the analysis), a solution will be computed as follows:

1. The direct BEM with the original source delivers the pressure distribution along the interface.
2. The pressure distribution is transformed into an equivalent point sources using Equation (11).
3. These point sources are used as input for a direct BEM model of the far field.

The prescription of point sources, which is necessary for the third step of the coupled solution for verification, is no problem when using the direct BEM (see Section 2).

For the actual hybrid method (BEM–coupling method–ray model) the third step is replaced by the ray method, which accounts for the refraction caused by meteorological inhomogeneity.

DOI: 10.1002/nme

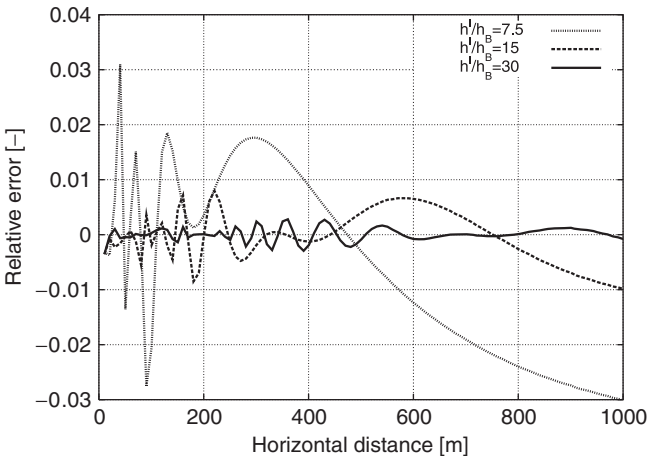

Figure 7. Decrease of the relative error of the coupling method for increasing interface heights h^{I} for constant barrier height h_{B}.

The relative error E_{rel} is defined as the relative difference of pressure amplitudes between the solution of the coupled model and the reference solution

$$E_{\mathrm{rel}} = \frac{|p_{\mathrm{coupled}}| - |p_{\mathrm{reference}}|}{|p_{\mathrm{reference}}|} \tag{12}$$

Obtained results show that the error depends on the size and the discretization of the interface and the frequency of the primary source. In Figure 7 the relative error is plotted as a function of the horizontal propagation distance for a barrier of height h_{B} in a 2D problem. The three curves represent different interface heights h^{I}. It can be observed that the increment of the interface height reduces the error significantly. This result is very important when estimating the discretization error when a reference solution is not available. It is shown for the present example that for an interface height relative to the barrier height $h^{\mathrm{I}}/h_{\mathrm{B}} = 30$ the error reduces to a few per mills.

Figure 9 shows results of a 3D example consisting of a rectangular sound barrier ($h_{\mathrm{B}} = 4$ m, $b_{\mathrm{B}} = 10$ m) and a point source of frequency $f = 100$ Hz located at $h_{\mathrm{S}} = 2$ m height and at a distance $d_{\mathrm{S}} = 2$ m in front of the barrier. Two sizes and two discretization strategies for the interface were used. The small interface possesses a length of $L = 30$ m and a height of $H = 20$ m, while the large one is of length $L = 60$ m and $H = 40$ m high (see Figure 8). The coarse discretization for the interface consists in a maximum distance between points $t_{\max} = 0.4$ m, while for the fine discretization the maximum distance between the points is reduced to $t_{\max} = 0.2$ m. Three solutions were considered: the small interface with the coarse discretization (results labelled as 'small, coarse'), the small interface with the fine discretization (results labelled 'small, fine') and the large interface with the coarse discretization (results labelled as 'large, coarse').

The goal of this parameter variation is to study the computational effort (number of nodes and elements used in the interface discretization) necessary to achieve prescribed error level. Taking as reference the solution obtained using the small interface and the coarse discretization, the error reduction is estimated using two improved models which represent the same increment in the

DOI: 10.1002/nme

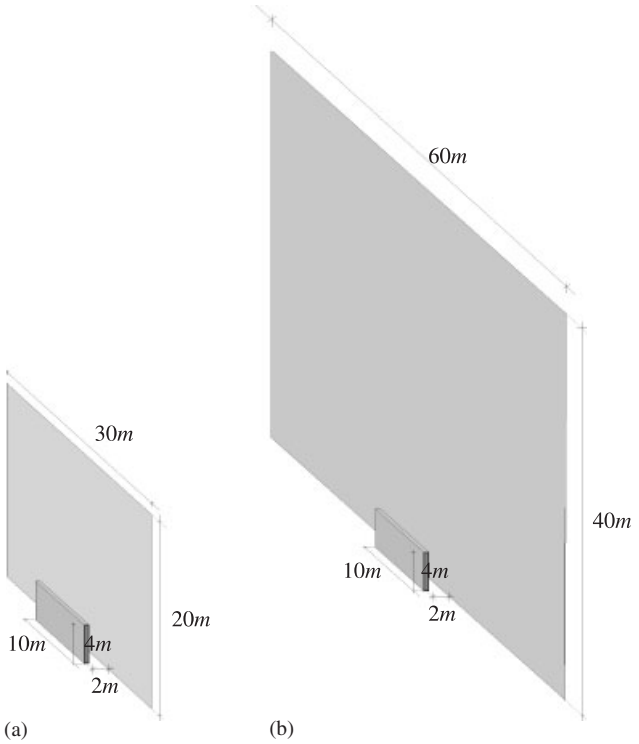

Figure 8. Test configuration with (a) small and (b) large interface.

computational effort: the finer discretization (the distance between the points is halved) and a larger interface (the size of the interface doubled). From the results in Figure 9 it can be observed that the finer grid does not lead to a significant improvement of the error, although the number of elements is four times higher than in before. On the other hand, an enlargement of the interface size delivers much better results. Similar results were obtained for other analysis performed for different frequencies of the point source. From the whole of computed results, it can be stated that a discretization refinement beyond the $\lambda/6$-rule (minimum six element per wave length) does not lead to mentionable error reduction, whereas an extension of the interface size is the more efficient way to reduce the error.

4.2. Coupling by the method of fundamental solutions (MFS)

The advantages of the MFS are its properties as a meshless method: neither the domain, nor the boundary of the model have to be discretized. These characteristics of the method will result in the fact that when used as a coupling procedure between BEM and the raytracing method, no integration along the auxiliary interface will be needed.

The idea of the MFS is to place a number of sources around the domain Ω of interest such that the given boundary conditions on the boundary Γ are fulfilled. The number of boundary points is M, the number of sources is N. Each source delivers a contribution to the sound pressure at point i,

DOI: 10.1002/nme

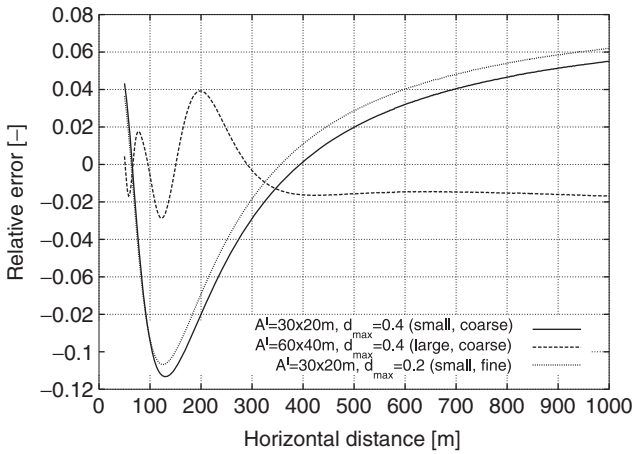

Figure 9. Relative error for three different discretizations of the interfaces: $A^{\mathrm{I}} = 30\ \mathrm{m} \times 20\ \mathrm{m}$, $d_{\max} = 0.4\ \mathrm{m}$ (small, coarse); $A^{\mathrm{I}} = 60\ \mathrm{m} \times 40\ \mathrm{m}$, $d_{\max} = 0.4\ \mathrm{m}$ (large, coarse); $A^{\mathrm{I}} = 30\ \mathrm{m} \times 20\ \mathrm{m}$, $d_{\max} = 0.2\ \mathrm{m}$ (small, fine).

which corresponds to the fundamental solution $G(x_i, \xi_j)$ weighted by an intensity factor a_j. The approximate solution then results as linear superposition of all contributions $j = 1, 2, \ldots, N$:

$$\sum_{j=1}^{N} G(x_i, \xi_j) a_j = p(x_i), \quad x_i \in \Omega, \quad \xi_i \in \bar{\Omega} \tag{13}$$

Equation (13) is formulated as boundary condition by inserting the known boundary values $\bar{p}_i$ at the boundary point i on the right-hand side. Setting up this boundary condition for all M boundary points leads to a linear system of equations

$$\mathbf{A} \cdot \mathbf{x} = \mathbf{b} \tag{14}$$

where the matrix entries A_{ij} represent the influence of a point source with unit intensity at location ξ_j on the field point at x_i, i.e.

$$A_{ij} = G(x_i, \xi_j) \tag{15}$$

The solution vector $\mathbf{x}$ contains the unknown source intensities a_j, the vector $\mathbf{b}$ contains the prescribed boundary values.

The number of sources N does not have to be equal to the number of boundary points M, but can also be lower. In this case, an equation system with a non-square matrix is yielded. It represents a linear least-squares problem which can be solved using the singular value decomposition method. The matrix $\mathbf{A}$ is decomposed into a product of three matrices:

$$\mathbf{A} = \mathbf{U} \cdot \mathbf{S} \cdot \mathbf{V}' \tag{16}$$

DOI: 10.1002/nme

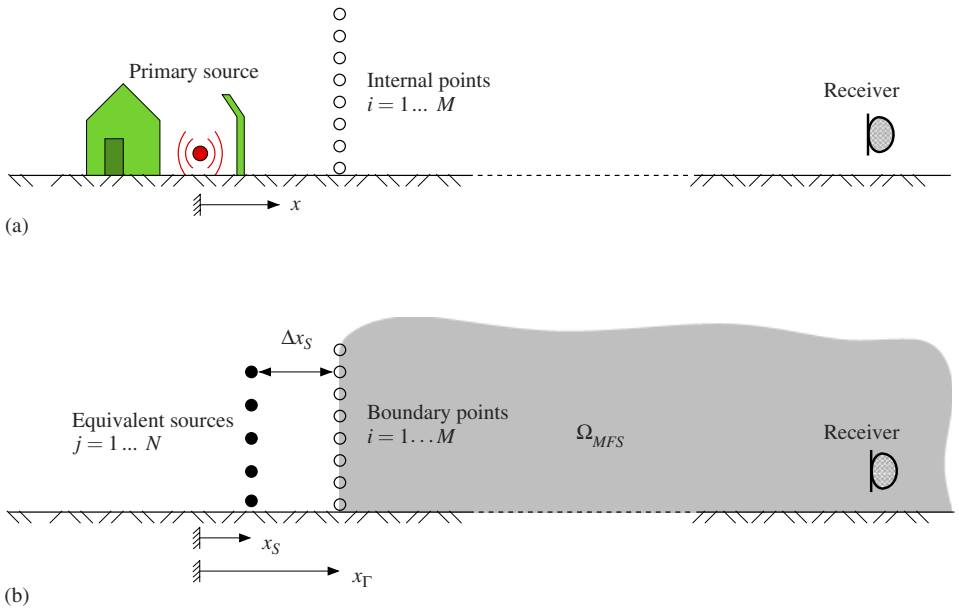

Figure 10. Sketch of the MFS geometry for the special coupling problem with fixed source positions: (a) configuration for BEM and (b) configuration for MFS.

$\mathbf{U}$ is a $(M \times N)$-matrix, whereas $\mathbf{V}'$ represents a square $(N \times N)$-matrix. The columns of both these matrices are orthonormal, i.e. it holds

$$\mathbf{U^{-1}} = \mathbf{U^T}, \quad \mathbf{V^{-1}} = \mathbf{V^T} \tag{17}$$

where $\mathbf{U^{-1}}$ is the pseudo-inverse of $(M \times N)$-matrix $\mathbf{U}$. $\mathbf{S}$ is a diagonal matrix of dimension $(N \times N)$ and contains the eigenvalues s_{ii} of $\mathbf{A}$ on its principle diagonal. With the decomposition of $\mathbf{A}$, for the inverse $\mathbf{A}^{-1}$ it follows

$$\mathbf{A^{-1}} = \mathbf{V} \cdot \mathrm{diag}(s_{ii}) \cdot \mathbf{U} \tag{18}$$

which is used to compute the solution $\mathbf{x}$.

An advantage of this method is its ease of implementation as part of a computer program. Optionally, for the choice of the best positions of the equivalent sources, an optimization algorithm can be applied in order to minimize the residual at the prescribed boundary points [23, 29].

The idea behind the coupling procedure is illustrated in Figure 10. It is proposed to approximate the near field by a number of sources (•) using the MFS. It is postulated that the sound pressure at the boundary points (○) has to match the results from a direct BEM calculation with primary source and discretized obstacles. The arrangement of the MFS sources and the boundary points is generally arbitrary. However, it has to be ensured that the sources are placed in the near field, so that the complete effect of refraction is taken into account during the ray calculation. The arrangement of the sources and the boundary points in vertical lines (or in 3D in a vertical surface) turns out to be suitable. Some more general studies to optimize the location of the source points are performed in [23]. The points are here distributed in an equidistant manner. The vertical line

DOI: 10.1002/nme

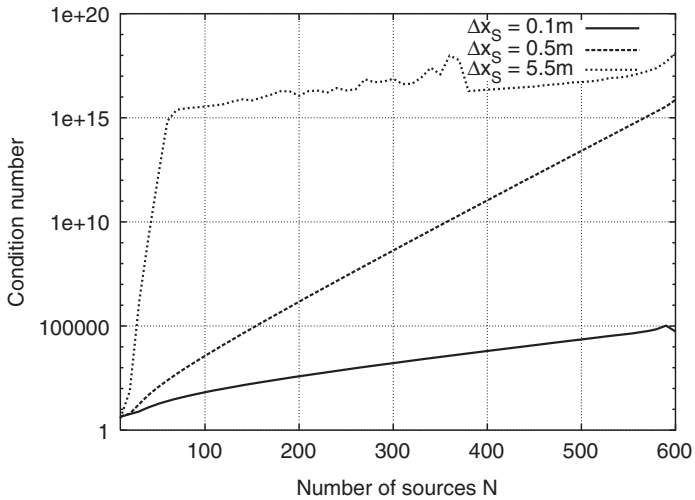

Figure 11. Condition number of the system matrix depending on the number of sources; different source positions: $\Delta x_S = 0.1$, 0.5 and 5.5 m.

of boundary points in Figure 10(b) can be considered as the boundary of the far field, i.e. of the domain where the ray method is applied.

Figure 11 shows the condition number of matrix **A** as a function of the number of sources N. The three curves represent different source positions, which are lined up vertically according to the boundary points. The number of boundary points is fixed at $M = 600$. They are distributed equally over a height of 60 m, i.e. a distance of 0.1 m between points. The sources are placed at the same relative distance, every 0.1 m. So, the height of the source array depends on the number of sources N. The x-position of the boundary points is fixed at $x_\Gamma = 10.5$ m. Only the horizontal distance Δx_S between the N source points and the M boundary points is varied and must be greater than zero to avoid singularities. The results show very different condition numbers for the three considered source positions. If the sources are—relative to the distance between two points—too far from the boundary points, the system of equations is very ill-conditioned. However, if they are placed too closely, the values of the matrix entries become very large (singularity for $r \to 0$). The condition number of matrix **A** increases with the number of sources and depends strongly on the source position s.

The accuracy of the coupling method is assessed following a procedure similar to that used in Section 4.1. In this way, a problem with a homogeneous atmosphere is considered and the results from the coupled BEM-Raytracing analysis are compared to those obtained using a BEM reference solution for the complete problem. The number of boundary points $M = 600$ and the number of point sources $N = 200$ are chosen for the MFS coupling procedure.

In order to emphasize the effect of the condition number on the quality of the solution, the same three positions for the source points reported in Figure 11 are considered. The resulting relative error results (see Equation (12)) are presented in Figure 12 as a function of the distance from the primary source. A distance up to 1000 m is considered.

The error analysis shows that for all three curves, i.e. for different source positions, the error vanishes at the first point ($x = 0$). This behaviour is because at this point the fulfilment of the

DOI: 10.1002/nme

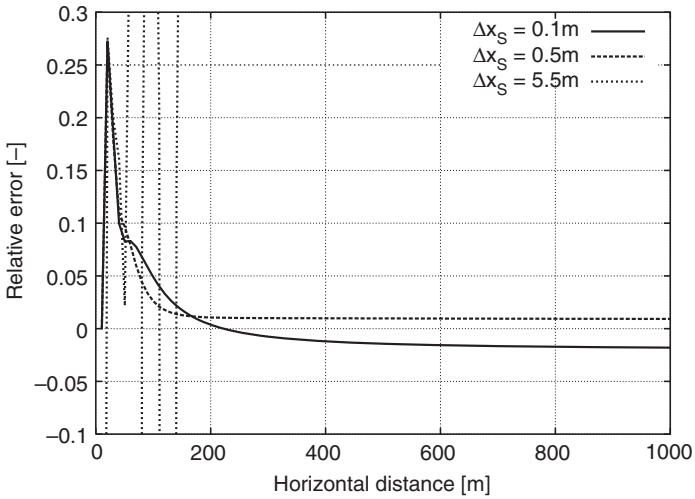

Figure 12. Relative error at internal points for different source positions: $\Delta x_S = 0.1$, 0.5 and 5.5 m.

boundary condition was enforced in the couple procedure. From this point on, the three sets of results can be classified into two groups. On the one hand, the error curves for the source positions $x_S = 0.1$ m and $x_S = 0.5$ m present a nice behaviour. While the error is sporadically above 25% for distances up to 100 m, it dramatically reduces for distances greater to 200 m to achieve values in the range from 1 to 2% and then it remains constant. These error levels were checked for distances up to 10 000 m (not shown in Figure 12). On the other hand, the source position $x_S = 5.5$ m produces unusable results which oscillate and diverge with the increment of the distance. This behaviour is a consequence of the very high condition number of the **A** matrix, of about $10E+16$ (see Figure 11 for $x_S = 5.5$ m and $N = 200$).

5. APPLICATION TO OUTDOOR SOUND PROPAGATION

In this section, the focus lies on outdoor sound propagation problems as shown in Figure 13. An important aspect in any example is to distinguish between the near field and the far field of the primary source. The near field is a very small area compared to the complete domain considered. Besides the primary source, i.e. the physically present sound source, it also encloses obstacles, which are situated in the immediate neighbourhood and thus have a large influence on the sound propagation. The goal of analysing these problems is to determine the resulting sound field at points of interest in the far field. In practice, this can be residential areas or other sensible locations for which in the computation model a receiver point is placed. The receiver points usually are at a distance of about 100–1000 m.

The effect of meteorological influences—as implemented in the coupled model—is stronger for larger distances. Thus, for the large distance propagation the ray model that is used includes the effect of refraction due to a wind or temperature profile. The near field, in which diffraction and multiple reflections occur due to a complex geometry, is calculated with the direct BEM, which considers these phenomena implicitly.

DOI: 10.1002/nme

Figure 13. Typical problem in outdoor sound propagation.

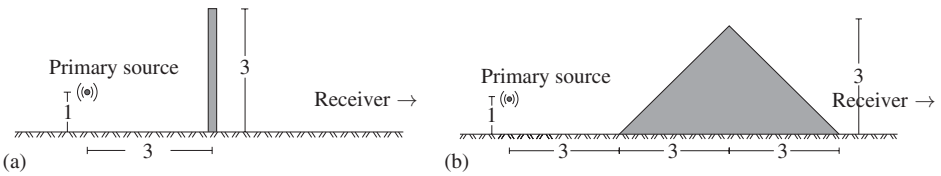

Figure 14. Cross-sections of the considered noise protection constructions; dimensions in [m].

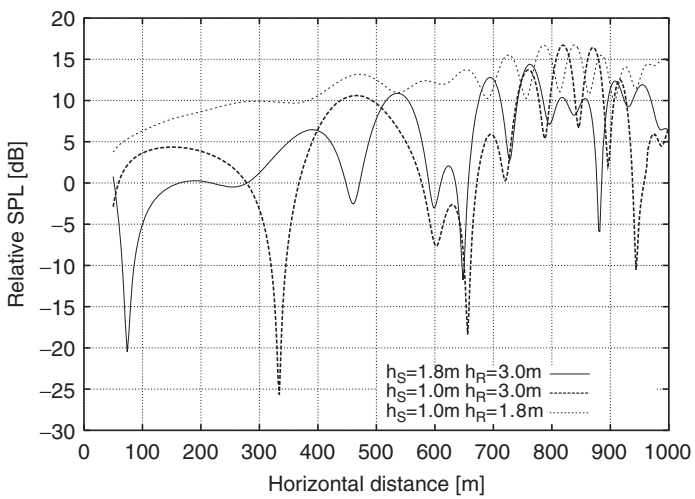

Figure 15. Refracting atmosphere ($a = c'_{\text{eff}}(z) = 0.1\ \text{s}^{-1}$) over rigid ground without an obstacle; three combinations of source heights h_{S} and receiver heights h_{R}.

Here, the performance of a sound barrier and a noise protection dam is analysed and compared. The cross-section of both the 3D constructions is shown in Figure 14. The length of wall and dam in the third direction is $l = 5$ m, such that additional diffraction around the sides of the constructions can be expected. The receiver points are placed at $h_{\text{R}} = 1.6$ m height up to 1000 m from the source.

For the refracting atmosphere, a linear sound speed profile is applied with $c_0 = 340\,\text{m/s}$ on the ground and a vertical gradient $a = 0.1\ \text{s}^{-1}$. For the simulation with a homogeneous atmosphere a simple BEM calculation is performed, whereas for the simulation with a refracting atmosphere the coupled BEM–ray tracing model *via* the IBEM procedure presented above is used. The interface for the indirect BEM is discretized as a rectangle of $l \times h = 15\,\text{m} \times 10\,\text{m}$. The computation time for

DOI: 10.1002/nme

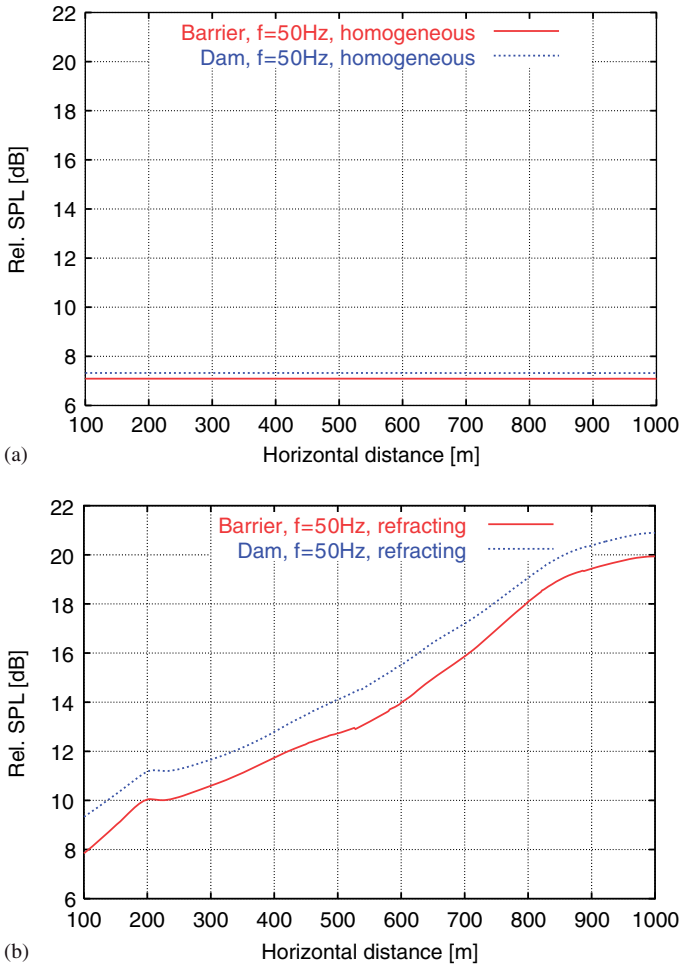

Figure 16. Performance of the barrier and the dam in two different atmospheric conditions; relative SPL (resp. free space) for $f = 50$ Hz: (a) homogeneous atmosphere and (b) downward refracting atmosphere.

the direct BEM calculation in the first step is between 2 and 5 min on a SUN Spark III 900 MHz processor. Similar computing times were necessary for the IBEM coupling procedure.

All result plots show the relative sound pressure level (Rel. SPL), which is in this case related to the sound pressure in homogeneous free space, i.e. without ground and other geometry. In Figure 15, the situation without an obstacle is analysed by varying the source and receiver heights. The curves show that zones of destructive interference arise due to refraction. For the lowest receiver height $h_R = 1.8$ m this interference effect is less distinctive, but the sound pressure level is generally higher because the energy focuses near the ground.

The performance of the sound barrier and the dam as noise reduction measures is shown in Figure 16 for a frequency of $f = 50$ Hz and in Figure 17 for $f = 500$ Hz. It can be seen for both the frequencies, that the case with a downward refracting atmosphere (Figures 16(b) and 17(b))

DOI: 10.1002/nme

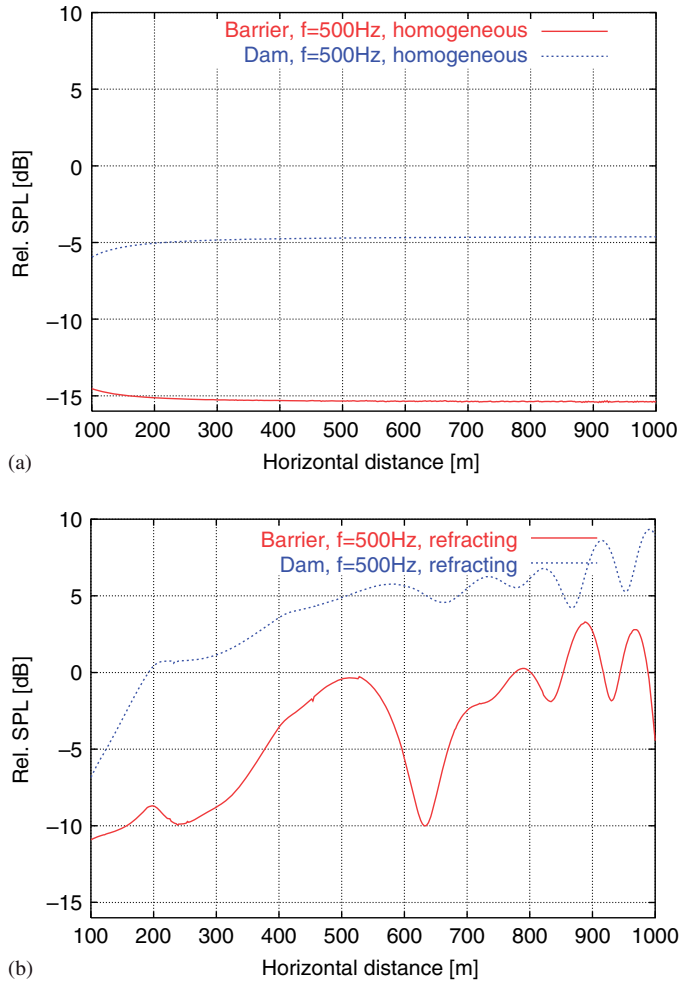

Figure 17. Performance of the barrier and the dam in two different atmospheric conditions; relative SPL (resp. free space) for $f = 500$ Hz: (a) homogeneous atmosphere and (b) downward refracting atmosphere.

leads to higher sound pressure levels compared to the homogeneous medium (Figures 16(a) and 17(a)). The effect of refraction increases with the horizontal distance from the source. For the high frequency (Figure 17) lower relative sound pressure levels occur, because diffraction effects are low and thus the performances of both measures are more efficient than for low frequencies. Furthermore, it can be observed that for low frequency the barrier and the dam have approximately the same reduction effect, whereas for high frequency the screening effect of the sound barrier is much better than the dam due to the shorter distance from the top of the construction to the sound source.

Similar applications on the performance of sound barriers and dams as shown in this section, but without the effect of refraction, are investigated in [14].

DOI: 10.1002/nme

6. CONCLUSIONS

In this paper, the coupling of the BEM and a raytracing method for solving outdoor acoustics was presented. These methods were chosen in order to better represent the propagation phenomena which are dominant in the different parts of the domain: the BEM to model diffraction in the near field close to the noise source, and the ray method to model refraction in the far field. It was shown that the problem can be divided into two parts in which the BEM and the ray method are applied, respectively. Both numerical methods were briefly described highlighting their main characteristics, advantages and aspects concerning the coupling.

Two alternative approaches were developed for the coupling procedure, which are based on the indirect BEM and the MFS, respectively. Both approaches were implemented and verified using reference solutions for the homogeneous (no refraction) test problems. The developed methodology was successfully applied to solve an application problem.

The hybrid method represents diffraction and refraction. Hence, it is advantageous compared to the detached use of raytracing or BEM and it is also superior compared to the BEM using subdomain techniques, that is restricted to a constant speed of sound per subdomain. With the hybrid method, an inhomogeneous propagation medium with a speed of sound gradient can be handled.

REFERENCES

1. Embleton TFW. Tutorial on sound propagation outdoors. *Journal of the Acoustical Society of America* 1996; **100**(1):31–48.
2. Piercy JE, Embleton TFW, Sutherland LC. Review of noise propagation in the atmosphere. *Journal of the Acoustical Society of America* 1977; **61**(6):1403–1418.
3. Salomons EM. *Computational Atmospheric Acoustics*. Kluwer: Dordrecht, 2001.
4. Walker R. Acoustic modelling—approximations to the real world. *White Paper WHP 005*, BBC, 2001.
5. Cederfeldt L. *On the Use of Finite Element Method on Some Acoustical Problems*. Swedish Council for Building Research, Stockholm, 1979.
6. Langer S, Antes H. Analyses of sound transmission through windows by coupled finite and boundary element methods. *Acta Acustica united with Acustica* 2003; **89**:78–85.
7. Sommerfeld A. *Partielle Differentialgleichungen in der Physik*. Verlag Harri Deutsch: Frankfurt, 1978.
8. Blumrich R, Heimann D. Numerical estimation of atmospheric approximation effects in outdoor sound propagation modelling. *Acta Acustica* 2004; **90**:24–37.
9. van Renterghem T, Botteldooren D. Numerical simulation of the effect of trees in downwind noise barrier performance. *Acta Acustica united with Acustica* 2003; **89**:764–778.
10. Björk EA. A simple statistical curved ray model for noise under downward refracting conditions. *Acta Acustica* 2005; **91**:389–391.
11. Li KM, Taherzadeh S, Attenborough K. An improved ray-tracing algorithm for predicting sound propagation outdoors. *Journal of the Acoustical Society of America* 1998; **104**(4):2077–2083.
12. Salomons EM. Downwind propagation of sound in an atmosphere with a realistic sound-speed profile: a semianalytical ray model. *Journal of the Acoustical Society of America* 1994; **95**(5):2425–2436.
13. Antes H. Anwendungen der Methode der Randelemente in der Elastodynamik und der Fluidmechanik. *Mathematische Methoden in der Technik*, vol. 9. Teubner: Stuttgart, 1988.
14. Antes H. Applications in environmental noise. *Boundary Element Methods in Acoustics* (Chapter 6). Springer: Berlin, 1991; 225–260.
15. von Estorff O. *Boundary Elements in Acoustics*. WIT Press: Southampton, 2000.
16. Wu TW. *Boundary Element Acoustics—Fundamentals and Computer Codes*. WIT Press: Northampton, 2001.
17. de Lacerda LA, Wrobel LC, Mansur WJ. A boundary integral formulation for two/dimensional acoustic radiation in a subsonic uniform flow. *Journal of the Acoustical Society of America* 1996; **100**:31–48.

DOI: 10.1002/nme

18. Tsuji T, Tsuchiya T, Kagawa Y. Finite element and boundary element modelling for acoustic wave transmission in mean flow medium. *Journal of Sound and Vibration* 2002; **255**:849–866.
19. Wu TW, Lee L. A direct boundary element integral formulation for acoustic radiation in a subsonic uniform flow. *Journal of Sound and Vibration* 1994; **175**:51–63.
20. Fischer M, Gaul L. Application of the fast BEM for structural-acoustic simulations. *Journal of Computational Acoustics* 2005; **13**(1):87–98.
21. Fairweather G, Karageoghis A, Martin PA. The method of fundamental solutions for scattering and radiation problems. *Engineering Analysis with Boundary Elements* 2003; **27**:759–769.
22. Ochmann M. The complex equivalent source method for sound propagation over an impedance plane. *Journal of the Acoustical Society of America* 2004; **116**(6):3304–3311.
23. Cisilino AP, Sensale B. Optimal placement of the source points for singular problems in the method of fundamental solutions. *Advances in Boundary Element Techniques*, vol. II. Hoggar Press: Geneva, 2001.
24. Zhang P, Wu TW, Lee L. A coupled FEM/BEM formulation for acoustic radiation in a subsonic non/uniform flow. *Journal of Sound and Vibration* 1996; **192**:333–347.
25. Premat E, Defrance J, Priour M, Aballea F. Coupling BEM and GFPE for complex outdoor sound propagation. *Proceedings of Euronoise 2003*, Naples, Italy, 2003.
26. Beer G. *Programming the Boundary Element Method—An Introduction for Engineers*. Wiley: New York, Berlin, 2001.
27. Hampel S, Langer S, Cisilino AP. Kopplung von BEM und Strahlenverfahren mit Hilfe der Methode der Fundamentallösungen. *Fortschritte in der Akustik*, *DAGA '06*, Braunschweig, Germany, 2006.
28. Langer S, Hampel S. Coupling boundary elements to a ray tracing procedure using the singular indirect method. *Proceedings in Applied Mathematics and Mechanics* (*PAMM*), *Gesellschaft für Angewandte Mathematik und Mechanik* 2005; **5**(1):609–610.
29. Hampel S. *Numerische Simulation der Schallausbreitung unter Berücksichtigung meteorologischer Einflüsse*, Braunschweiger Schriften zur Mechanik, Mechanik-Zentrum, Technische Universität Braunschweig, 2006.

DOI: 10.1002/nme